Check for updates

Abstract and Applied Analysis

WILEY

RESEARCH ARTICLE OPEN ACCESS

Optimal Control and Global Sensitivity Analysis of a Multiroute Zika Transmission Model With Wolbachia

Abdoulaye Sow[1] | Cherif Diallo[1] | Hocine Cherifi[2]

[1]Department of Computer Science, Algebra Laboratory Cryptography Codes and Applications, Gaston Berger University, Saint-Louis, Senegal | [2]Department of Computer Science, ICB UMR 6303 CNRS Université Bourgogne Europe, Dijon, France

Correspondence: Abdoulaye Sow (sow.abdoulaye6@ugb.edu.sn)

Received: 21 November 2025 | **Revised:** 6 April 2026 | **Accepted:** 30 April 2026

Academic Editor: AbdelMaksoud Soliman

Keywords: mathematical modeling | optimal control | sensitivity analysis | sexual transmission | vector-borne transmission | vertical transmission | Wolbachia | Zika virus

ABSTRACT

The Zika virus exhibits complex transmission dynamics involving vector-borne, sexual, and vertical pathways, which complicates the design of effective control strategies. In this work, we develop an integrated SICR–SI mathematical model coupling human and mosquito populations, incorporating Wolbachia-based biocontrol, sexual prevention, and vector control as intervention strategies. The model parameters are calibrated using epidemiological time-series data from seven Pacific island archipelagos, and the basic reproduction number R_0 is analytically derived. Our results show that Wolbachia substantially reduces the vector component of transmission but cannot eliminate Zika in the presence of sexual transmission, which maintains a residual epidemic risk. We demonstrate that combining Wolbachia releases with sexual prevention yields a synergistic reduction in incidence greater than the sum of their individual effects. Using optimal control theory, we identify time-dependent intervention strategies that minimize both infection burden and implementation costs. A global sensitivity analysis (Sobol indices) highlights the dominant influence of mosquito-related parameters and Wolbachia coverage on epidemic outcomes. Overall, this study underscores the necessity of multitarget and coordinated intervention strategies to effectively reduce Zika transmission and its severe neurological complications.

1 | Introduction

The Zika virus, primarily transmitted by mosquitoes of the Aedes genus, emerged as a global health threat during the 2015–2016 outbreak. In addition to vector-borne transmission, the virus can also spread through sexual and vertical routes, complicating its dynamics and control [1, 2]. These multiple transmission pathways, combined with the risk of severe neurological complications such as microcephaly in newborns, underscore the need for mathematical models that can accurately capture the complex epidemiology of the virus [3, 4].

Several studies have addressed Zika modeling by integrating one or more transmission routes. For example [3], developed a model accounting for sexual and vertical transmission, while [5, 6] analyzed the impact of sexual transmission on epidemic dynamics. Other studies, such as [7], introduced optimal control strategies to limit spread. Work by Biswas et al. [8, 9] also explored the effects of vertical transmission and sexual behavior on virus dynamics.

Furthermore, the use of mosquitoes infected with the Wolbachia bacterium has shown promise in reducing the vector competence

This is an open access article under the terms of the Creative Commons Attribution License, which permits use, distribution and reproduction in any medium, provided the original work is properly cited.

Copyright © 2026 Abdoulaye Sow et al. *Abstract and Applied Analysis* published by John Wiley & Sons Ltd.

of Aedes mosquitoes, as demonstrated by Guo et al. [10–12]. Studies by Walker et al. [13, 14] demonstrated the invasion potential and persistence of Wolbachia strains in mosquito populations. Recent studies, such as [15, 16], have further confirmed the effectiveness of this approach under field conditions, while [17] provided a comprehensive review of Wolbachia-based strategies.

Vertical transmission in mosquitoes, an important mechanism for virus persistence, has been documented by Zimler and Alto [18], and the implications of sexual transmission for control have been emphasized by Moreira et al. [19, 20]. However, few models have simultaneously integrated all three transmission routes vector-borne, sexual, and vertical—and evaluated the combined effect of multiple control strategies, particularly the release of Wolbachia-infected mosquitoes, sexual prevention, and conventional vector control. Moreover, the analysis of synergy between these interventions and the identification of the most influential parameters via global sensitivity methods remain underexplored.

In this work, we propose a deterministic SICR-SI model that couples human and vector dynamics and integrates all three transmission routes along with three control levers. We estimate parameters using epidemiological data from seven archipelagos, compute the basic reproduction number R_0, and study the impact of Wolbachia coverage. Finally, we formulate and solve an optimal control problem aimed at minimizing both disease incidence and intervention costs, and we identify key parameters via Sobol sensitivity analysis.

This global approach aims to inform public health decisions by quantifying the relative effectiveness and complementarity of available strategies to combat the Zika virus, in line with recent work on integrated arbovirus modeling [21].

The remainder of this article is organized as follows. In Section 2, we present the formulation of the proposed SICR–SI model and describe the underlying assumptions. Section 3 is devoted to the mathematical analysis of the model, including well-posedness, the derivation of the basic reproduction number, and stability results. In Section 4, we perform parameter estimation and assess the model's fit to epidemiological data. Section 5 explores the impact of Wolbachia-based interventions and analyzes the sensitivity of key parameters. In Section 6, we formulate and solve the optimal control problem and evaluate different intervention strategies. Finally, Section 7 concludes the article with a discussion of the main findings and perspectives for future research.

2 | Model Formulation

We consider a deterministic compartmental model describing the transmission dynamics of the Zika virus, integrating vector-borne, sexual, and vertical transmission pathways, as well as the effects of three control strategies: the release of Wolbachia-infected mosquitoes, sexual prevention, and vector control. The model links the human and mosquito populations through a system of ordinary differential equations.

The total human population N_H is divided into two subgroups: women of reproductive age (indexed by F) and the general population (indexed by G). Each subgroup is structured into four compartments: susceptible (S), infected (I), individuals with severe neurological complications (C), and recovered (R):

$$N_H = S_F + I_F + C_F + R_F + S_G + I_G + C_G + R_G.$$

The total mosquito population N_M consists of two subpopulations wild mosquitoes (S_w, I_w) and Wolbachia-infected mosquitoes (S_b, I_b):

$$N_M = S_w + I_w + S_b + I_b.$$

Vector transmission depends on mosquito–human contact, while sexual transmission acts directly between infected and susceptible individuals. The force of infection for vector-borne transmission is defined as follows:

$$\lambda_m = \beta_H \frac{I_w + \delta I_b}{N_M},$$

where β_H is the transmission rate from mosquitoes to humans, and $\delta < 1$ represents the reduction in vector competence due to Wolbachia.

To improve the realism of the sexual transmission component, we allow for heterogeneous transmission patterns between subpopulations by distinguishing the direction of contacts. Rather than assuming uniform mixing, we introduce different transmission rates to capture possible asymmetries in interactions between the considered groups.

Accordingly, we define the following forces of infection:

$$\lambda_{s,F} = \beta_{s,\mathrm{FG}} \frac{I_G + C_G}{N_H},$$

$$\lambda_{s,G} = \beta_{s,\mathrm{GF}} \frac{I_F + C_F}{N_H} + \beta_{s,\mathrm{GG}} \frac{I_G + C_G}{N_H},$$

where $\beta_{s,FG}$ is the sexual transmission rate from infected general population (men) to susceptible women, $\beta_{s,GF}$ is the transmission rate from infected women to susceptible general population (men), and $\beta_{s,GG}$ is the transmission rate from infected general population to susceptible general population (men-to-men). This structure reflects that women can only be infected sexually by men, while men can be infected by both women and men.

The control parameters u, v, and $w \in [0, 1]$ represent as follows:

1. the proportion of mosquitoes infected with Wolbachia (u),
2. the reduction in sexual transmission rates (v), and
3. the reduction in vector transmission due to vector control (w).

All sexual transmission rates are reduced by the same factor $(1 - v)$, reflecting a general reduction in sexual contact or transmission probability.

4058, 2026, 1, Downloaded from https://onlinelibrary.wiley.com/doi/10.1155/aaa/1574642 by Senegal Hinari NPL, Wiley Online Library on [22/06/2026]. See the Terms and Conditions (https://onlinelibrary.wiley.com/terms-and-conditions) on Wiley Online Library for rules of use; OA articles are governed by the applicable Creative Commons License

2.1 | Human Population

$$\begin{aligned}
\frac{dS_F}{dt} &= \Lambda_{HF} - (1-w)\lambda_m S_F - (1-v)\lambda_{s,F} S_F - \mu_H S_F,\\
\frac{dI_F}{dt} &= (1-w)\lambda_m S_F + (1-v)\lambda_{s,F} S_F - (\gamma + \kappa + \mu_H) I_F,\\
\frac{dC_F}{dt} &= \kappa I_F - (\gamma + \alpha + \mu_H) C_F,\\
\frac{dR_F}{dt} &= \gamma(I_F + C_F) - \mu_H R_F,\\
\frac{dS_G}{dt} &= \Lambda_{HG} - (1-w)\lambda_m S_G - (1-v)\lambda_{s,G} S_G - \mu_H S_G,\\
\frac{dI_G}{dt} &= (1-w)\lambda_m S_G + (1-v)\lambda_{s,G} S_G - (\gamma + \kappa + \mu_H) I_G,\\
\frac{dC_G}{dt} &= \kappa I_G - (\gamma + \alpha + \mu_H) C_G,\\
\frac{dR_G}{dt} &= \gamma(I_G + C_G) - \mu_H R_G.
\end{aligned} \tag{1}$$

2.2 | Mosquito Population

$$\begin{aligned}
\frac{dS_w}{dt} &= \Lambda_M(1-u) - (1-w)\beta_M \frac{I_F + \theta C_F + I_G + \theta C_G}{N_H} S_w - \mu_M S_w,\\
\frac{dI_w}{dt} &= (1-w)\beta_M \frac{I_F + \theta C_F + I_G + \theta C_G}{N_H} S_w - \mu_M I_w,\\
\frac{dS_b}{dt} &= \Lambda_M u - \delta(1-w)\beta_M \frac{I_F + \theta C_F + I_G + \theta C_G}{N_H} S_b - \mu_M S_b,\\
\frac{dI_b}{dt} &= \delta(1-w)\beta_M \frac{I_F + \theta C_F + I_G + \theta C_G}{N_H} S_b - \mu_M I_b.
\end{aligned} \tag{2}$$

where $\theta \in [0,1]$ represents the relative infectiousness of individuals with neurological complications (C_F, C_G) compared to those in the infectious class (I_F, I_G). For the baseline analysis, we assume $\theta = 1$, acknowledging that the infectious potential of this group is not fully established. This parameter can be explored in sensitivity analyses.

The transmission pathways of the Zika virus considered in this study are illustrated in Figure 1. A schematic representation of the full model structure, including all compartments and control strategies, is provided in Figure 2.

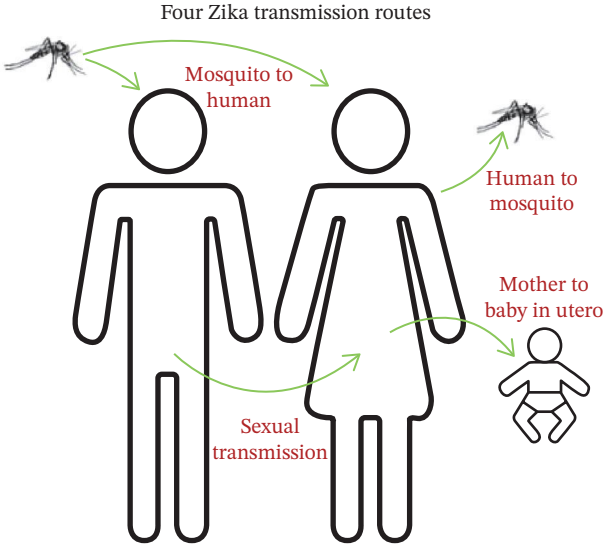


FIGURE 1 | Transmission pathways of the Zika virus.

This system couples the human and vector dynamics and captures the key mechanisms of transmission. It accounts for the vector-borne transmission, modulated by w, which represents the effectiveness of vector control measures; the sexual transmission, reduced by v; the reduction in vector competence induced by Wolbachia infection, represented by the parameters u and δ.

3 | Model Analysis

3.1 | Existence, Positivity, and Boundedness of Solutions

In this section, we establish the mathematical well-posedness of the system (1)–(2) by proving the existence, uniqueness, positivity, and boundedness of solutions. These properties ensure that the model is biologically consistent.

3.1.1 | Invariant Region and Notation

Let the total human and mosquito populations be denoted by $N_H(t)$ and $N_M(t)$, respectively, where:

$$\begin{aligned}
N_H &= S_F + I_F + C_F + R_F + S_G + I_G + C_G + R_G,\ N_M\\
&= S_w + I_w + S_b + I_b.
\end{aligned} \tag{3}$$

The dynamics of the system are analyzed in the feasible region $\Omega \subset \mathbb{R}^{12}_+$, defined as follows:

$$\Omega = \left\{ (S_F, \ldots, I_b) \in \mathbb{R}^{12}_+ : N_H \le \frac{\Lambda_H}{\mu_H},\ N_M \le \frac{\Lambda_M}{\mu_M} \right\}, \tag{4}$$

where $\Lambda_H = \Lambda_{HF} + \Lambda_{HG}$.

3.1.2 | Positivity of Solutions

To ensure the biological relevance of the model, we first show that all state variables remain nonnegative for all $t \ge 0$.

Lemma 1. *Let the initial conditions be nonnegative. Then, the solutions $(S_F, \ldots, I_b)$ of the system (1)–(2) remain in $\mathbb{R}^{12}_+$ for all $t > 0$.*

Proof. Consider the equation for the susceptible human population S_F:

$$\frac{dS_F}{dt} = \Lambda_{HF} - \left[(1-w)\lambda_m + (1-v)\lambda_{s,F} + \mu_H\right] S_F \ge -\Phi(t) S_F, \tag{5}$$

where $\Phi(t) = (1-w)\lambda_m(t) + (1-v)\lambda_{s,F}(t) + \mu_H$. By integration, we obtain:

$$S_F(t) \ge S_F(0) \exp\left(-\int_0^t \Phi(\tau) d\tau \right) > 0. \tag{6}$$

Similarly, for the infected compartment I_F:

$$\frac{dI_F}{dt} \ge -(\gamma + \kappa + \mu_H) I_F \Longrightarrow I_F(t) \ge I_F(0) e^{-(\gamma+\kappa+\mu_H)t} \ge 0. \tag{7}$$

Applying the same comparison principle to all other human and mosquito compartments, it follows that all state variables remain nonnegative for all $t \ge 0$. □

4058, 2026, 1, Downloaded from https://onlinelibrary.wiley.com/doi/10.1155/aaa/1574642 by Senegal Hinari NPL, Wiley Online Library on [22/06/2026]. See the Terms and Conditions (https://onlinelibrary.wiley.com/terms-and-conditions) on Wiley Online Library for rules of use; OA articles are governed by the applicable Creative Commons License

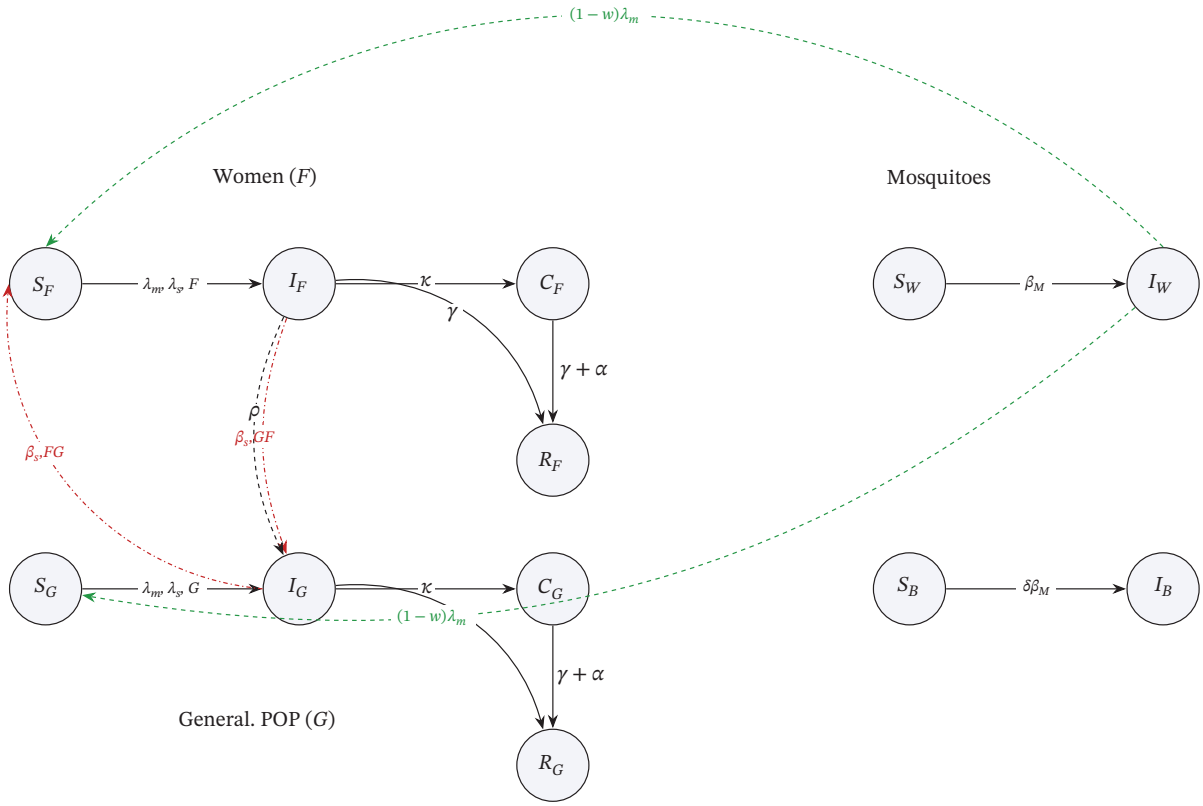


FIGURE 2 | Schematic diagram of the Zika virus transmission model. The human population is divided into two subgroups: women (F) and general population (G), each stratified into susceptible (S_F, S_G), infected (I_F, I_G), complication (C_F, C_G), and recovered (R_F, R_G) compartments. The mosquito population is divided into two classes: mosquitoes carrying Wolbachia (S_w, I_w) and those without Wolbachia (S_b, I_b). Zika virus transmission occurs through two main routes vector-borne transmission with force of infection λ_m, and sexual transmission with force of infection λ_s. The transmission rates between humans and mosquitoes are denoted by β_M and $\delta\beta_M$, while β_s^{FG} and β_s^{GF} represent sexual transmission between subpopulations. The progression to complications is governed by κ, recovery occurs at rate γ, and disease-induced mortality is represented by α. Control measures are incorporated through three parameters: u (Wolbachia deployment), v (sexual transmission prevention), and w (vector control), which reduce the effective transmission rates.

3.1.3 | Boundedness and Invariance

Lemma 2. *The region Ω is positively invariant and attracting for the system (1)–(2).*

Proof. Summing the equations for the human population yields:

$$\frac{dN_H}{dt} = \Lambda_H - \mu_H N_H - \alpha(C_F + C_G) \le \Lambda_H - \mu_H N_H. \tag{8}$$

According to the comparison theorem, $N_H(t) \le N_H(0)e^{-\mu_H t} + \frac{\Lambda_H}{\mu_H}(1 - e^{-\mu_H t})$. Thus, $lim\ sup_{t\to\infty} N_H(t) \le \frac{\Lambda_H}{\mu_H}$.

For the mosquito population, the total dynamics follow:

$$\frac{dN_M}{dt} = \Lambda_M - \mu_M N_M \Longrightarrow N_M(t) = \frac{\Lambda_M}{\mu_M} + \left(N_M(0) - \frac{\Lambda_M}{\mu_M}\right)e^{-\mu_M t}. \tag{9}$$

As $t \to \infty$, $N_M(t) \to \frac{\Lambda_M}{\mu_M}$. If $N_M(0) = \Lambda_M/\mu_M$, then $N_M(t) = \Lambda_M/\mu_M$ for all $t \ge 0$. Consequently, Ω is an attracting and positively invariant set. □

3.2 | Existence and Uniqueness

Theorem 1. *For any initial condition in Ω, there exists a unique global solution to the system (1)–(2) for all $t \ge 0$.*

Proof. The right-hand side of the system (1)–(2) is a vector field $f(x)$. Since the forces of infection $\lambda_m, \lambda_{s,F}$, and $\lambda_{s,G}$ are ratios with denominators N_M and N_H, they are continuously differentiable provided $N_M, N_H > 0$. Since the solutions remain in the positively invariant region $\Omega \subset \mathbb{R}^{12}_+$, and the right-hand side of the system consists of smooth functions for nonnegative arguments, the vector field is locally Lipschitz continuous in Ω. Thus, the vector field is locally Lipschitz continuous on Ω. By the Cauchy-Lipschitz theorem, a unique local solution exists. Since Ω is compact (all variables are bounded), this solution is global in time. □

3.3 | Disease-Free Equilibrium (DFE)

The DFE of the system (1)–(2) is obtained by setting all infection-related compartments to zero and solving for the remaining variables. At the DFE, we have:

$$I_F = C_F = R_F = I_G = C_G = R_G = I_w = I_b = 0,$$

4058, 2026, 1, Downloaded from https://onlinelibrary.wiley.com/doi/10.1155/aaa/1574642 by Senegal Hinari NPL, Wiley Online Library on [22/06/2026]. See the Terms and Conditions (https://onlinelibrary.wiley.com/terms-and-conditions) on Wiley Online Library for rules of use; OA articles are governed by the applicable Creative Commons License

and the susceptible compartments satisfy:

$$\frac{dS_F}{dt} = \Lambda_{HF} - \mu_H S_F = 0 \Rightarrow S_F^0 = \frac{\Lambda_{HF}}{\mu_H},$$
$$\frac{dS_G}{dt} = \Lambda_{HG} - \mu_H S_G = 0 \Rightarrow S_G^0 = \frac{\Lambda_{HG}}{\mu_H},$$
$$\frac{dS_w}{dt} = \Lambda_M(1-u) - \mu_M S_w = 0 \Rightarrow S_w^0 = \frac{\Lambda_M(1-u)}{\mu_M},$$
$$\frac{dS_b}{dt} = \Lambda_M u - \mu_M S_b = 0 \Rightarrow S_b^0 = \frac{\Lambda_M u}{\mu_M}.$$

Thus, the DFE is given by:

$$\mathscr{E}_0 = \left(S_F^0, 0, 0, 0, S_G^0, 0, 0, 0, S_w^0, 0, S_b^0, 0\right).$$

3.4 | Basic Reproduction Number

The basic reproduction number R_0 represents the average number of secondary infections generated by a single infectious individual in a completely susceptible population. We compute R_0 using the next-generation matrix method [22].

The infectious compartments relevant for disease transmission are:

- Infected humans: I_F, C_F, I_G, C_G
- Infected mosquitoes: I_w and I_b

The total infectious pressure from humans for the mosquito infection is given by $I_H = I_F + \theta C_F + I_G + \theta C_G$, where θ accounts for the relative infectiousness of the complications class.

We consider the vector of infected states:

$$\mathbf{x} = (I_F, C_F, I_G, C_G, I_w, I_b)^\top.$$

At the DFE, we have:

$$N_H^0 = S_F^0 + S_G^0 = \frac{\Lambda_{HF} + \Lambda_{HG}}{\mu_H},\ N_M^0 = S_w^0 + S_b^0 = \frac{\Lambda_M}{\mu_M}.$$

The total susceptible human population at DFE is $S_H^0 = S_F^0 + S_G^0 = N_H^0$.

The forces of infection at the DFE become:

$$\lambda_m^0 = \beta_H \frac{I_w + \delta I_b}{N_M^0},\ \lambda_{s,F}^0 = \beta_{s,FG} \frac{I_G + C_G}{N_H^0},$$
$$\lambda_{s,G}^0 = \beta_{s,GF} \frac{I_F + C_F}{N_H^0} + \beta_{s,GG} \frac{I_G + C_G}{N_H^0}.$$

Following the next-generation matrix approach, we write:

$$\frac{d\mathbf{x}}{dt} = (\mathscr{F} - \mathscr{V})\mathbf{x},$$

where $\mathscr{F}$ contains the terms representing new infections and $\mathscr{V}$ contains the transition terms (including recovery, mortality, and progression).

Given the structure of the model, we can reduce the system by noting that the total infectious pressure from humans for the vector infection is:

$$H_I = I_F + \theta C_F + I_G + \theta C_G.$$

Using the relationships $S_F^0/N_H^0 = \Lambda_{HF}/(\Lambda_{HF} + \Lambda_{HG})$ and $S_G^0/N_H^0 = \Lambda_{HG}/(\Lambda_{HF} + \Lambda_{HG})$, we define the effective sexual transmission parameters:

$$\beta_s^F = \beta_{s,FG},$$

$$\beta_s^G = \beta_{s,GF} \frac{\Lambda_{HF}}{\Lambda_{HF} + \Lambda_{HG}} + \beta_{s,GG} \frac{\Lambda_{HG}}{\Lambda_{HF} + \Lambda_{HG}}.$$

The reduction to a single parameter β_s in the R_0 expression that follows is a simplifying assumption made due to data limitations. In the full model, sexual transmission involves distinct rates $\beta_{s,FG}$, $\beta_{s,GF}$, and $\beta_{s,GG}$. Under the assumption of symmetric mixing and using the effective parameters β_s^F and β_s^G defined above, we approximate the sexual component by a single effective rate β_s. The resulting R_0 formula should therefore be interpreted as an approximation that captures the main qualitative behavior.

The reduced new infection matrix for the states (H_I, I_w, I_b) is:

$$F = \begin{pmatrix} (1-v)\beta_s & \beta_H \frac{S_H^0}{N_M^0} & \delta\beta_H \frac{S_H^0}{N_M^0} \\ \beta_M \frac{S_w^0}{N_H^0} & 0 & 0 \\ \delta\beta_M \frac{S_b^0}{N_H^0} & 0 & 0 \end{pmatrix}.$$

The transition matrix is:

$$V = \begin{pmatrix} \gamma + \mu_H & 0 & 0 \\ 0 & \mu_M & 0 \\ 0 & 0 & \mu_M \end{pmatrix}.$$

The next-generation matrix is $K = FV^{-1}$:

$$K = \begin{pmatrix} \frac{(1-v)\beta_s}{\gamma + \mu_H} & \frac{\beta_H S_H^0}{N_M^0 \mu_M} & \frac{\delta\beta_H S_H^0}{N_M^0 \mu_M} \\ \frac{\beta_M S_w^0}{N_H^0(\gamma + \mu_H)} & 0 & 0 \\ \frac{\delta\beta_M S_b^0}{N_H^0(\gamma + \mu_H)} & 0 & 0 \end{pmatrix}.$$

The characteristic equation of K is:

$$\det(K - \lambda I) = -\lambda\left[\lambda^2 - \frac{(1-v)\beta_s}{\gamma + \mu_H}\lambda - \frac{\beta_H \beta_M S_H^0 S_w^0}{N_M^0 N_H^0 \mu_M(\gamma + \mu_H)}\left(1 + \delta^2 \frac{S_b^0}{S_w^0}\right)\right] = 0.$$

The spectral radius $\rho(K)$ is the largest positive root of:

$$\lambda^2 - \frac{(1-v)\beta_s}{\gamma + \mu_H}\lambda - \frac{\beta_H \beta_M S_H^0 S_w^0}{N_M^0 N_H^0 \mu_M(\gamma + \mu_H)}\left(1 + \delta^2 \frac{S_b^0}{S_w^0}\right) = 0.$$

4058, 2026, 1, Downloaded from https://onlinelibrary.wiley.com/doi/10.1155/aaa/1574642 by Senegal Hinari NPL, Wiley Online Library on [22/06/2026]. See the Terms and Conditions (https://onlinelibrary.wiley.com/terms-and-conditions) on Wiley Online Library for rules of use; OA articles are governed by the applicable Creative Commons License

Substituting $S_H^0 = N_H^0$, $S_w^0/N_M^0 = 1-u$, and $S_b^0/S_w^0 = u/(1-u)$:

$$\frac{\beta_H\beta_M S_H^0 S_w^0}{N_M^0 N_H^0 \mu_M}\left(1+\delta^2\frac{S_b^0}{S_w^0}\right) = \frac{\beta_H\beta_M(1-u)}{\mu_M}\left(1+\delta^2\frac{u}{1-u}\right) = \frac{\beta_H\beta_M}{\mu_M}((1-u)+\delta^2 u).$$

Thus, the quadratic equation becomes:

$$\lambda^2 - \frac{(1-v)\beta_s}{\gamma+\mu_H}\lambda - \frac{\beta_H\beta_M}{\mu_M(\gamma+\mu_H)}((1-u)+\delta^2 u) = 0.$$

Solving this quadratic and taking the positive root, the basic reproduction number is:

$$R_0 = \frac{1}{2(\gamma+\mu_H)}\left[(1-v)\beta_s + \sqrt{((1-v)\beta_s)^2 + 4(\gamma+\mu_H)\frac{\beta_H\beta_M}{\mu_M(\gamma+\mu_H)}((1-u)+\delta^2 u)}\right].$$

Given that $S_H^0 = N_H^0$ and $S_w^0/N_M^0 = (1-u)$, the final expression for R_0 can be written in a compact and standard form:

$$R_0 = \frac{R_s + \sqrt{R_s^2 + 4R_m^2}}{2},$$

where:

$$R_s = \frac{(1-v)\beta_s}{\gamma+\mu_H}\ (\text{sexual transmission component}),$$

$$R_m = \sqrt{\frac{\beta_H\beta_M}{\mu_M(\gamma+\mu_H)}((1-u)+\delta^2 u)}\ (\text{vector-borne component}).$$

This decomposition shows that the overall reproduction number arises from a nonlinear interaction between the contributions of vector-borne and sexual transmission pathways. The vector-borne component decreases with increasing Wolbachia coverage u (since $\delta<1$), while the sexual transmission component decreases with the level of sexual prevention v.

3.5 | Stability Analysis

This section is devoted to the stability analysis of the DFE of system (1)–(2). We first investigate the local stability using linearization techniques, and then establish the global stability by applying the approach of Castillo-Chavez et al. [23].

3.6 | Local Stability of the DFE

The local stability of the DFE, denoted by $\mathscr{E}_0$, is determined by the eigenvalues of the Jacobian matrix evaluated at $\mathscr{E}_0$.

Theorem 2. (Local stability of the DFE). *The DFE $\mathscr{E}_0$ of system (1)–(2) is locally asymptotically stable if $R_0<1$, and unstable if $R_0>1$.*

Proof. Linearizing the system around

$$\mathscr{E}_0 = \left(S_F^0, 0, 0, 0, S_G^0, 0, 0, 0, S_w^0, 0, S_b^0, 0\right),$$

the Jacobian matrix takes a block triangular form:

$$J(\mathscr{E}_0) = \begin{pmatrix} J_{SS} & J_{SI} \\ 0 & J_{II} \end{pmatrix}.$$

The eigenvalues of J_{SS} are $-\mu_H$ (with multiplicity four) and $-\mu_M$ (with multiplicity two), which are strictly negative. Therefore, the stability is governed by the infected subsystem J_{II}.

The characteristic polynomial of J_{II} can be written as:

$$P(\lambda) = (\lambda+\gamma+\alpha+\mu_H)^2(\lambda+\mu_M)^2(\lambda^2+a_1\lambda+a_2).$$

Clearly, four eigenvalues are negative. For the remaining quadratic term, we apply the Routh–Hurwitz criterion:

$$a_1 = \mu_M+\gamma+\mu_H > 0,\ a_2 = \mu_M(\gamma+\mu_H)(1-R_0).$$

If $R_0<1$, then $a_2>0$, implying that both roots have negative real parts. Hence, $\mathscr{E}_0$ is locally asymptotically stable. If $R_0>1$, then $a_2<0$, and at least one eigenvalue is positive, implying instability. □

3.7 | Global Stability of the DFE

To establish global stability, we rewrite the system as:

$$\begin{cases} \dfrac{dX}{dt} = F(X,Z), \\ \dfrac{dZ}{dt} = G(X,Z),\ G(X,0)=0, \end{cases} \tag{10}$$

where

$$X = (S_F, R_F, S_G, R_G, S_w, S_b)^T,\ Z = (I_F, C_F, I_G, C_G, I_w, I_b)^T.$$

Theorem 3. (Global stability of the DFE). *The DFE $\mathscr{E}_0$ is globally asymptotically stable in Ω if $R_0<1$ and the following conditions hold:*

(H1) *The subsystem $\frac{dX}{dt} = F(X,0)$ has a globally asymptotically stable equilibrium X^*.*

(H2) *$G(X,Z) = AZ - \widehat{G}(X,Z)$, where $\widehat{G}(X,Z)\geq 0$ for all $(X,Z)\in\Omega$, and $A = D_Z G(X^*,0)$ is an M-matrix.*

3.7.1 | Verification of (H1)

When $Z=0$, the subsystem reduces to:

$$\frac{dS_F}{dt} = \Lambda_{HF} - \mu_H S_F,\ \frac{dS_G}{dt} = \Lambda_{HG} - \mu_H S_G,$$

4058, 2026, 1, Downloaded from https://onlinelibrary.wiley.com/doi/10.1155/aaa/1574642 by Senegal Hinari NPL, Wiley Online Library on [22/06/2026]. See the Terms and Conditions (https://onlinelibrary.wiley.com/terms-and-conditions) on Wiley Online Library for rules of use; OA articles are governed by the applicable Creative Commons License

$$\frac{dS_w}{dt} = \Lambda_M(1-u) - \mu_M S_w,\ \frac{dS_b}{dt} = \Lambda_M u - \mu_M S_b.$$

All these equations are linear and admit globally asymptotically stable equilibria:

$$S_F^0 = \frac{\Lambda_{HF}}{\mu_H},\ S_G^0 = \frac{\Lambda_{HG}}{\mu_H},\ S_w^0 = \frac{\Lambda_M(1-u)}{\mu_M},\ S_b^0 = \frac{\Lambda_M u}{\mu_M}.$$

Thus, condition (H1) holds.

3.7.2 | Verification of (H2)

The Jacobian matrix of the infected subsystem at the DFE is:

$$A = \begin{pmatrix} -k_1 & 0 & 0 & 0 & \alpha_1 & \alpha_2 \\ \kappa & -k_2 & 0 & 0 & 0 & 0 \\ 0 & 0 & -k_1 & 0 & \alpha_3 & \alpha_4 \\ 0 & 0 & \kappa & -k_2 & 0 & 0 \\ \beta_1 & \beta_2 & \beta_1 & \beta_2 & -\mu_M & 0 \\ \beta_3 & \beta_4 & \beta_3 & \beta_4 & 0 & -\mu_M \end{pmatrix},$$

where $k_1 = \gamma + \kappa + \mu_H$ and $k_2 = \gamma + \alpha + \mu_H$.

Matrix A is a Metzler matrix with negative diagonal entries; hence it is a nonsingular M-matrix.

We now construct $\widehat{G}(X,Z)$ explicitly:

$$\widehat{G}(X,Z) = \begin{pmatrix} \widehat{G}_1 \\ 0 \\ \widehat{G}_3 \\ 0 \\ \widehat{G}_5 \\ \widehat{G}_6 \end{pmatrix},$$

where

$$\begin{aligned} \widehat{G}_1 &= (1-w)\beta_H(I_w + \delta I_b)\left(\frac{S_F^0}{N_M^0} - \frac{S_F}{N_M}\right) \\ &\quad + (1-v)\beta_{s,FG}(I_G + C_G)\left(\frac{S_F^0}{N_H^0} - \frac{S_F}{N_H}\right), \\ \widehat{G}_3 &= (1-w)\beta_H(I_w + \delta I_b)\left(\frac{S_G^0}{N_M^0} - \frac{S_G}{N_M}\right) \\ &\quad + (1-v)\beta_{s,GF}(I_F + C_F)\left(\frac{S_G^0}{N_H^0} - \frac{S_G}{N_H}\right), \\ \widehat{G}_5 &= \beta_M(I_F + I_G + C_F + C_G)\left(\frac{S_w^0}{N_H^0} - \frac{S_w}{N_H}\right), \\ \widehat{G}_6 &= \beta_M(I_F + I_G + C_F + C_G)\left(\frac{S_b^0}{N_H^0} - \frac{S_b}{N_H}\right). \end{aligned}$$

In the invariant region Ω, we have:

$$0 \le S_F \le S_F^0,\ 0 \le S_G \le S_G^0,\ 0 \le S_w \le S_w^0,\ 0 \le S_b \le S_b^0.$$

Thus,

$$\frac{S_F}{N_M} \le \frac{S_F^0}{N_M^0},\ \frac{S_G}{N_M} \le \frac{S_G^0}{N_M^0},\ \frac{S_w}{N_H} \le \frac{S_w^0}{N_H^0},\ \frac{S_b}{N_H} \le \frac{S_b^0}{N_H^0}.$$

Hence, all terms in parentheses are nonnegative, implying:

$$\widehat{G}(X,Z) \ge 0 \text{ for all } (X,Z) \in \Omega.$$

Therefore, condition (H2) is satisfied.

By the theorem of Castillo-Chavez et al. [23], the DFE $\mathscr{E}_0$ is globally asymptotically stable whenever $R_0 < 1$.

4 | Parameter Estimation and Model Fitting

The parameters of the SICR–SI model were estimated using weekly time series data of reported Zika virus cases from seven archipelagos: Tahiti, Leeward Islands, Moorea, Tuamotu–Gambier, Marquesas Islands, Austral Islands, and Yap. The datasets, obtained from official epidemiological reports of French Polynesia and the Federated States of Micronesia, cover the first epidemic wave (weeks 1–25), corresponding to the initial growth and peak phases of the outbreak.

For each locality, the available data consist of aggregated weekly reported cases. No disaggregated observations distinguishing between the two human subpopulations (F and G) were available. Consequently, the model was calibrated using total incidence data. The subdivision into F and G groups is therefore introduced at the modeling level to capture heterogeneity in transmission pathways, particularly in sexual contacts, and should be interpreted as a latent structure rather than directly observed compartments.

The key parameters estimated from the data include the vector-to-human transmission rate (β_M), the human-to-vector transmission rate (β_H), the effective sexual transmission rate (β_s), and the vertical transmission probability (ρ). Due to the lack of detailed behavioral or contact data, homogeneous and symmetric mixing was assumed for sexual transmission within and between the two subpopulations. Under this assumption, β_s represents an effective average transmission rate that aggregates all sexual contact patterns. This simplifying assumption ensures parameter identifiability while preserving the essential transmission mechanisms.

Parameter estimation was carried out by minimizing the nonlinear least squares error between the observed weekly incidence and the model-predicted incidence. Model trajectories were obtained by numerically integrating the system of differential Equations (1), (2). For each archipelago, the optimal parameter set was determined by maximizing the likelihood of observing the data given the model, while vector-related demographic parameters (mortality and incubation rates) were fixed based on values reported in the literature.

Uncertainty in parameter estimates was quantified by computing 95% confidence intervals using a bootstrap procedure with 500 resamplings. It is important to note that the use of aggregated data may limit the practical identifiability of certain parameters; therefore, the estimated values should be interpreted with caution, focusing primarily on qualitative insights and comparative dynamics rather than precise quantitative prediction.

Regarding Wolbachia-based interventions, no empirical deployment data were incorporated into the calibration procedure. Instead, Wolbachia-related parameters were introduced to explore hypothetical control scenarios and assess their potential impact on transmission dynamics. Consequently, simulations involving Wolbachia should be interpreted as exploratory.

Figure 3 provides a comprehensive assessment of the model performance across the seven archipelagos by jointly presenting the fitted epidemic curves and the associated residual diagnostics. Overall, the SICR–SI model successfully reproduces the temporal evolution of reported Zika cases in all locations.

4058, 2026, 1, Downloaded from https://onlinelibrary.wiley.com/doi/10.1155/aaa/1574642 by Senegal Hinari NPL, Wiley Online Library on [22/06/2026]. See the Terms and Conditions (https://onlinelibrary.wiley.com/terms-and-conditions) on Wiley Online Library for rules of use; OA articles are governed by the applicable Creative Commons License

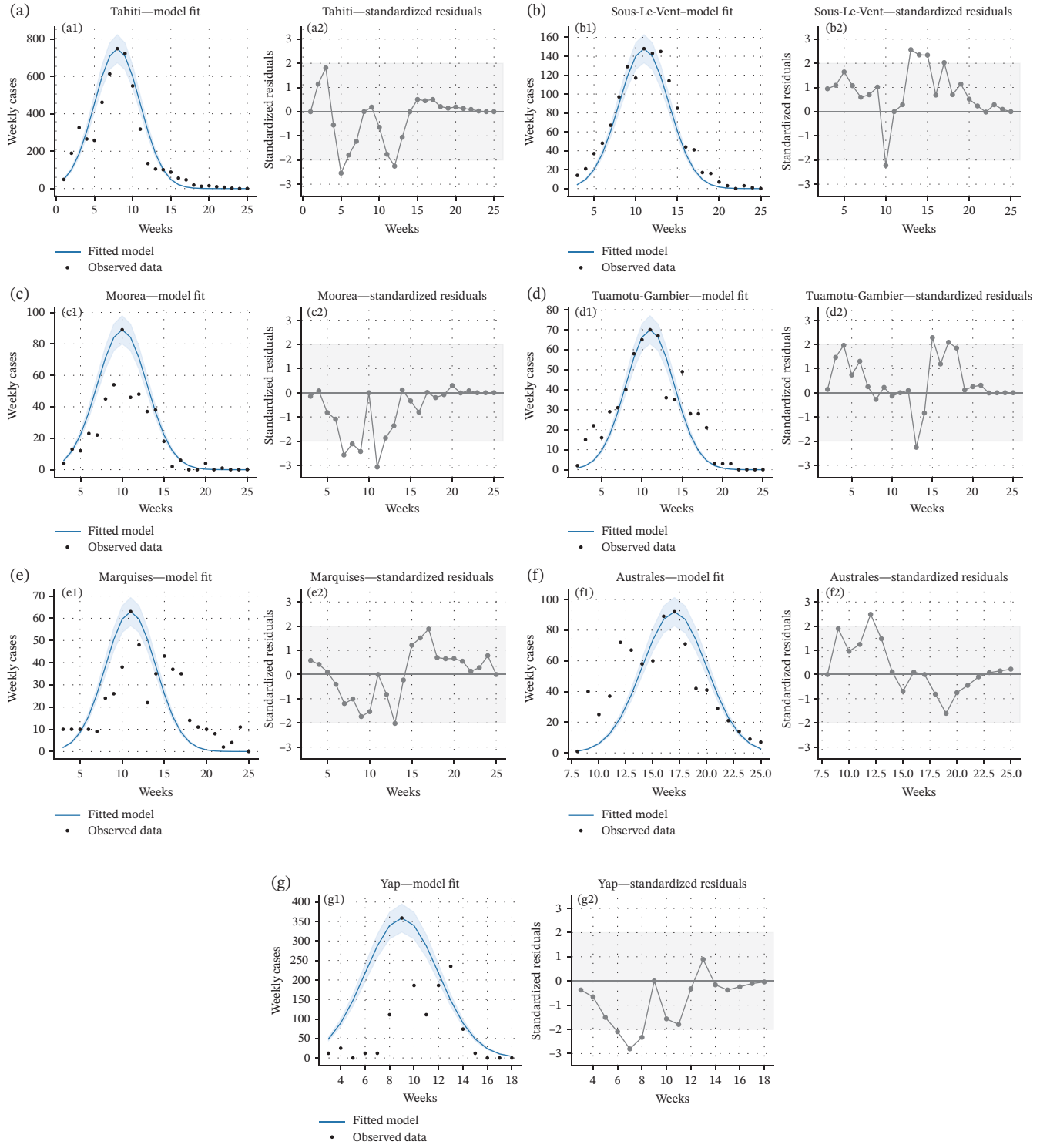


FIGURE 3 | Model SICR–SI fitting and residual analysis for each locality. Each subfigure shows two panels: (a1, b1, c1, d1, e1, f1, and g1) the comparison between observed cases (black dots) and the simulated curve (blue line, with a 95% confidence interval) and (a2, b2, c2, d2, e2, f2, and g2) the corresponding normalized residuals centered around zero, with a gray band indicating the $\pm 2\sigma$ interval. This combined representation provides an immediate visual assessment of the model fit quality and the temporal distribution of errors for each archipelago. (a) Tahiti, (b) Leeward Islands, (c) Moorea, (d) Tuamotu–Gambier Islands, (e) Marquesas Islands, (f) Austral Islands, and (g) Yap Island.

A very good agreement between model predictions and observed data is observed for Tahiti, the Leeward Islands, and Moorea, where both the timing and magnitude of the epidemic peaks are accurately captured. This indicates that the estimated transmission parameters adequately describe the dominant infection mechanisms in these relatively larger and more connected populations. The narrow confidence intervals further suggest limited uncertainty in parameter estimation for these regions.

For smaller or more isolated archipelagos, such as the Austral Islands and Yap, the model still captures the general epidemic trend, although slight discrepancies are observed. These deviations are likely attributable to stochastic effects, reporting variability, or

4058, 2026, 1, Downloaded from https://onlinelibrary.wiley.com/doi/10.1155/aaa/1574642 by Senegal Hinari NPL, Wiley Online Library on [22/06/2026]. See the Terms and Conditions (https://onlinelibrary.wiley.com/terms-and-conditions) on Wiley Online Library for rules of use; OA articles are governed by the applicable Creative Commons License

unmodeled local factors, which typically have a stronger influence in small population settings.

The residual analysis (Figure 3a2, b2, c2, d2, e2, f2, and g2) further supports the robustness of the model. Most normalized residuals lie within the $\pm 2\sigma$ interval and are symmetrically distributed around zero, indicating the absence of systematic bias. Moreover, no clear temporal structure or autocorrelation is detected, suggesting that the model adequately captures the main epidemic dynamics without omitting key mechanisms.

Occasional outliers, particularly in Yap and the Austral Islands, remain within expected statistical variability and do not indicate model misspecification. Such fluctuations are common in epidemiological data, especially when case numbers are low.

4.1 | Estimation of the Basic Reproduction Number

The basic reproduction number, R_0, was calculated from the fitted parameters according to the formula derived from the next-generation matrix.

The results, illustrated in Figure 4, reveal substantial spatial variability in R_0, ranging from 3.0 to 4.08 across the archipelagos. The highest values, observed in Moorea (4.08) and Yap (3.80), reflect favorable conditions for both vector-borne transmission (high *Aedes aegypti* density) and sexual transmission. Conversely, the lower values in the Australes (3.0) and Marquesas (3.02) archipelagos may be explained by reduced vector density and limited human mobility. The estimated parameters and the corresponding basic reproduction numbers R_0 are summarized in Table 1.

The results confirm that the SICR–SI model, calibrated with empirical data, successfully reproduces the spatio-temporal dynamics of the Zika virus. Residual analysis validates the statistical quality of the fit, while the R_0 estimates highlight geographic heterogeneity consistent with entomological and sociodemographic observations. These findings demonstrate the robustness of the model and support its use for prospective simulation of control scenarios, as presented in the following section.

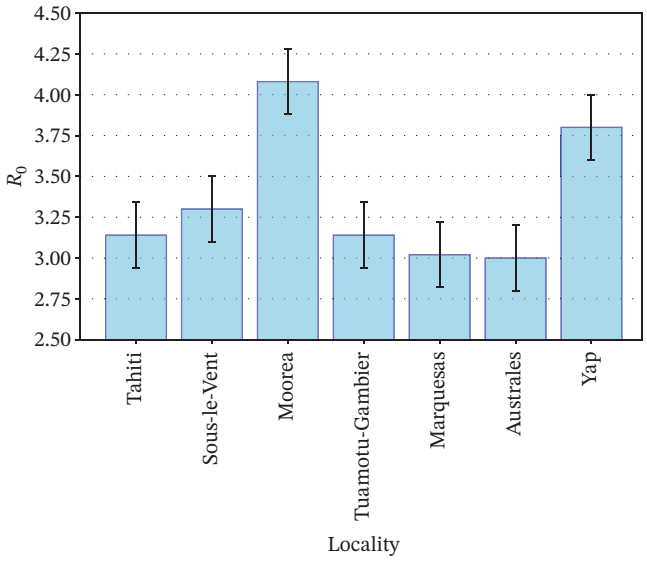


FIGURE 4 | Comparison of the basic reproduction number R_0 among localities. Error bars indicate 95% confidence intervals.

TABLE 1 | Estimated SCIR–SI model parameters for the seven localities studied.

Locality	β_H	β_M	β_s	ρ	R_0
Tahiti	0.61	0.61	0.216	0.23	3.14
Sous-le-Vent	0.67	0.51	0.216	0.083	3.30
Moorea	0.72	0.133	0.74	0.213	4.08
Tuamotu–Gambier	0.22	0.71	0.172	0.114	3.14
Marquesas	0.7	0.32	0.117	0.162	3.02
Australes	0.6	0.43	0.250	0.213	3.0
Yap	0.54	0.52	0.117	0.204	3.80

Note: Values in parentheses indicate 95% confidence intervals.

5 | Impact of Wolbachia on R_0

We analyzed the impact of Wolbachia introduction on Zika virus transmission dynamics by separately considering the vector (R_{0m}) and sexual (R_{0s}) components. Figure 5 shows the evolution of R_0 as a function of Wolbachia coverage $u \in [0, 1]$, assuming no sexual prevention ($v = 0$).

Without Wolbachia ($u = 0$), the basic reproduction number is high ($R_0 = 3.94$), with a majority contribution from vector transmission ($R_{0m} = 2.425$) and a nonnegligible sexual component ($R_{0s} = 0.35$). When Wolbachia reaches complete coverage ($u = 1$), the vector component is nearly eliminated ($R_{0m} = 0.242$), but the sexual component remains unchanged, leading to a residual R_0 of 2.472.

These results highlight a ceiling effect: Wolbachia effectively reduces vector transmission but does not modify sexual transmission, which limits its overall effectiveness. In the absence of sexual transmission, a critical threshold $u_c \approx 0.838$ is identified, corresponding to a minimum coverage of 83.8% required to achieve $R_0 < 1$ and eliminate the disease. In contrast, when sexual transmission is accounted for, no threshold appears in the interval $[0, 1]$: even complete Wolbachia coverage is insufficient to eradicate the epidemic.

These results suggest that Wolbachia deployment should be combined with other interventions targeting sexual transmission (prevention, screening, and awareness campaigns) and classical vector control to achieve optimal effectiveness.

6 | Optimal Control of the Zika Virus Transmission Model

This section presents the application of optimal control theory to the previously described Zika virus transmission model. The objective is to determine time-dependent control strategies that simultaneously minimize both the level of human and vector infection and the cost associated with health interventions. The three strategies considered are as follows: (i) the release of Wolbachia-infected mosquitoes (u), (ii) sexual prevention (v), and (iii) vector control (w). These controls are time-dependent functions, bounded in the interval $[0, 1]$, and act on vector reproduction, sexual transmission, and the mosquito–human contact probability, respectively.

4058, 2026, 1, Downloaded from https://onlinelibrary.wiley.com/doi/10.1155/aaa/1574642 by Senegal Hinari NPL, Wiley Online Library on [22/06/2026]. See the Terms and Conditions (https://onlinelibrary.wiley.com/terms-and-conditions) on Wiley Online Library for rules of use; OA articles are governed by the applicable Creative Commons License

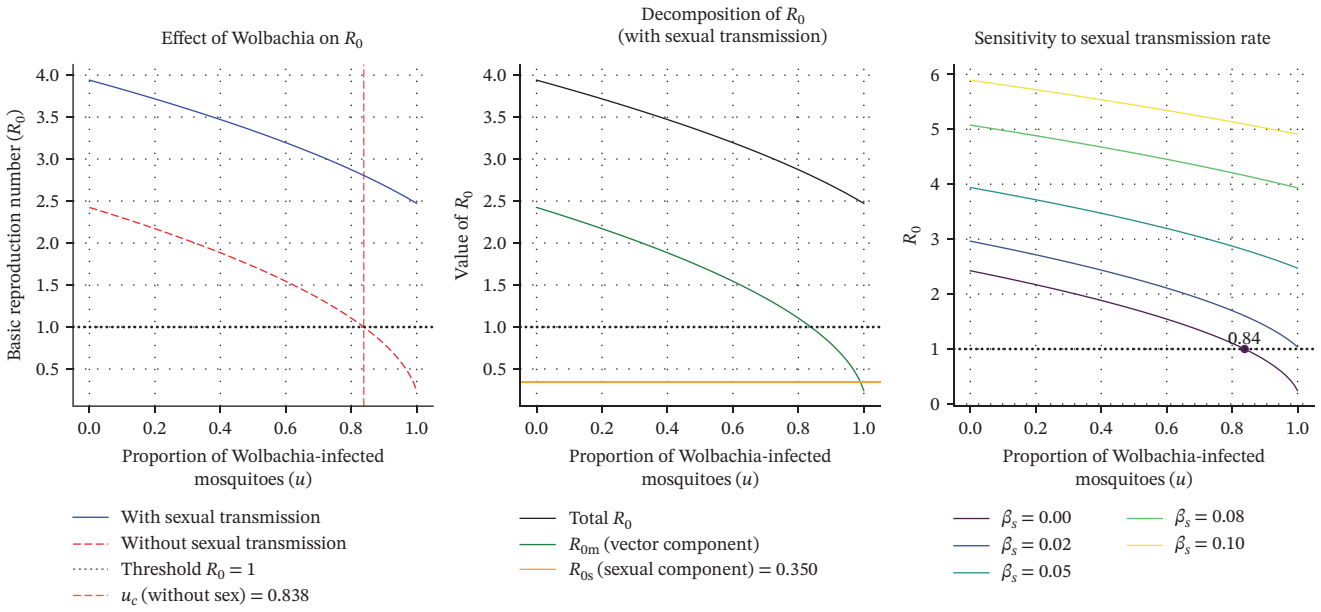


FIGURE 5 | Evolution of the basic reproduction number R_0 as a function of Wolbachia coverage u. The vector component R_{0m} (blue line) decreases strongly with u, while the sexual component R_{0s} (red line) remains constant. The black curve represents total R_0. The critical threshold $u_c = 0.838$ (dashed line) only exists when sexual transmission is absent.

6.1 | Formulation of the Optimal Control Problem

The state dynamical system is given by the differential Equations (1)–(2) describing the human population as follows:

$$(S_F, I_F, C_F, R_F, S_G, I_G, C_G, R_G),$$

and the vector population

$$(S_w, I_w, S_b, I_b),$$

under the influence of controls $u(t)$, $v(t)$, and $w(t)$.

The optimal control problem consists of minimizing the cost functional defined as follows:

$$J(u,v,w) = \int_0^T \left[A_1(C_F + C_G + I_F + I_G) + A_2(I_w + I_b) + \frac{1}{2}(D_1u^2 + D_2v^2 + D_3w^2)\right] dt, \tag{11}$$

where A_1 and A_2 are positive weights representing the severity of human and vector infections, while D_1, D_2, and D_3 weight the economic and operational costs associated with each control. The quadratic terms ensure the convexity of the functional.

The set of admissible controls is defined as follows:

$$U_{ad} = \{(u,v,w) \mid u,v,w \text{ measurable on } [0,T], \; 0 \le u(t), v(t), w(t) \le 1\}. \tag{12}$$

The optimal control problem is then formulated as follows:

$$\min_{(u,v,w)\in U_{ad}} J(u,v,w) \text{ subject to the dynamical system (1)– (2).}$$

To determine the necessary conditions for optimality, we introduce the Hamiltonian:

$$H = A_1(C_F + C_G + I_F + I_G) + A_2(I_w + I_b) + \frac{1}{2}(D_1u^2 + D_2v^2 + D_3w^2) + \sum_{j=1}^{12} \lambda_j f_j(S_F, I_F, C_F, R_F, S_G, I_G, C_G, R_G, S_w, I_w, S_b, I_b, u, v, w), \tag{13}$$

where the f_j are the right-hand sides of the state equations and the $\lambda_j(t)$ are the associated adjoint variables.

The adjoint vector satisfies the backward system as follows:

$$\frac{d\lambda_j}{dt} = -\frac{\partial H}{\partial y_j}, \; \lambda_j(T) = 0, \; j = 1, \ldots, 12,$$

where y_j denotes the j-th state variable.

The optimal controls u^*, v^*, and w^* are derived from the stationarity conditions $\partial H/\partial u = 0$, $\partial H/\partial v = 0$, and $\partial H/\partial w = 0$, leading to:

$$u(t) = \frac{\Lambda_M(\lambda_{S_b} - \lambda_{S_w})}{D_1}, \tag{14}$$

$$v(t) = \frac{\lambda_{s,F} S_F(\lambda_{S_F} - \lambda_{I_F}) + \lambda_{s,G} S_G(\lambda_{S_G} - \lambda_{I_G})}{D_2}, \tag{15}$$

$$w(t) = \frac{\lambda_m\left[S_F(\lambda_{S_F} - \lambda_{I_F}) + S_G(\lambda_{S_G} - \lambda_{I_G})\right] + \beta_M \frac{I_H}{N_H}\left[S_w(\lambda_{S_w} - \lambda_{I_w}) + \delta S_b(\lambda_{S_b} - \lambda_{I_b})\right]}{D_3}, \tag{16}$$

4058, 2026, 1, Downloaded from https://onlinelibrary.wiley.com/doi/10.1155/aaa/1574642 by Senegal Hinari NPL, Wiley Online Library on [22/06/2026]. See the Terms and Conditions (https://onlinelibrary.wiley.com/terms-and-conditions) on Wiley Online Library for rules of use; OA articles are governed by the applicable Creative Commons License

where $I_H = I_F + \theta C_F + I_G + \theta C_G$ and $N_b = S_b + I_b$.

Due to the bounds on the admissible controls, the actual optimal controls are given by the projection onto the interval $[0, 1]$:

$$u^*(t) = \max\left(0, \min\left(1, \frac{\Lambda_M\left(\lambda_{S_b} - \lambda_{S_w}\right)}{D_1}\right)\right), \tag{17}$$

$$v^*(t) = \max\left(0, \min\left(1, \frac{\lambda_{s,F} S_F\left(\lambda_{S_F} - \lambda_{I_F}\right) + \lambda_{s,G} S_G\left(\lambda_{S_G} - \lambda_{I_G}\right)}{D_2}\right)\right), \tag{18}$$

$$w^*(t) = \max\left(0, \min\left(1, \frac{\lambda_m\left[S_F\left(\lambda_{S_F} - \lambda_{I_F}\right) + S_G\left(\lambda_{S_G} - \lambda_{I_G}\right)\right] + \beta_M \frac{I_H}{N_H}\left[S_w\left(\lambda_{S_w} - \lambda_{I_w}\right) + \delta S_b\left(\lambda_{S_b} - \lambda_{I_b}\right)\right]}{D_3}\right)\right). \tag{19}$$

By differentiating the Hamiltonian with respect to each state variable, we obtain the system of backward adjoint equations:

$$\frac{d\lambda_{S_F}}{dt} = \left[(1-w)\lambda_m + (1-v)\lambda_{s,F} + \mu_H\right]\lambda_{S_F} - \left[(1-w)\lambda_m + (1-v)\lambda_{s,F}\right]\lambda_{I_F}, \tag{20}$$

$$\frac{d\lambda_{I_F}}{dt} = -A_1 + (\gamma + \kappa + \mu_H)\lambda_{I_F} - \kappa\lambda_{C_F} - \gamma\lambda_{R_F} - (1-\rho)\lambda_{S_G} - \rho\lambda_{I_G}, \tag{21}$$

$$\frac{d\lambda_{C_F}}{dt} = -A_1 + (\gamma + \alpha + \mu_H)\lambda_{C_F} - \gamma\lambda_{R_F}, \tag{22}$$

$$\frac{d\lambda_{R_F}}{dt} = \mu_H\lambda_{R_F}, \tag{23}$$

$$\frac{d\lambda_{S_G}}{dt} = \left[(1-w)\lambda_m + (1-v)\lambda_{s,G} + \mu_H\right]\lambda_{S_G} - \left[(1-w)\lambda_m + (1-v)\lambda_{s,G}\right]\lambda_{I_G}, \tag{24}$$

$$\frac{d\lambda_{I_G}}{dt} = -A_1 + (\gamma + \kappa + \mu_H)\lambda_{I_G} - \kappa\lambda_{C_G} - \gamma\lambda_{R_G} - \frac{\partial\lambda_{s,F}}{\partial I_G}(1-v)S_F\left(\lambda_{S_F} - \lambda_{I_F}\right) - \frac{\partial\lambda_{s,G}}{\partial I_G}(1-v)S_G\left(\lambda_{S_G} - \lambda_{I_G}\right), \tag{25}$$

$$\frac{d\lambda_{C_G}}{dt} = -A_1 + (\gamma + \alpha + \mu_H)\lambda_{C_G} - \gamma\lambda_{R_G} - \frac{\partial\lambda_{s,F}}{\partial C_G}(1-v)S_F\left(\lambda_{S_F} - \lambda_{I_F}\right) - \frac{\partial\lambda_{s,G}}{\partial C_G}(1-v)S_G\left(\lambda_{S_G} - \lambda_{I_G}\right), \tag{26}$$

$$\frac{d\lambda_{R_G}}{dt} = \mu_H\lambda_{R_G}, \tag{27}$$

$$\frac{d\lambda_{S_w}}{dt} = \left[(1-w)\beta_M\frac{I_H}{N_H} + \mu_M\right]\lambda_{S_w} - (1-w)\beta_M\frac{I_H}{N_H}\lambda_{I_w}, \tag{28}$$

$$\frac{d\lambda_{I_w}}{dt} = (-A_2 + \mu_M)\lambda_{I_w}, \tag{29}$$

$$\frac{d\lambda_{S_b}}{dt} = \left[\delta(1-w)\beta_M\frac{I_H}{N_H} + \mu_M\right]\lambda_{S_b} - \delta(1-w)\beta_M\frac{I_H}{N_H}\lambda_{I_b}, \tag{30}$$

$$\frac{d\lambda_{I_b}}{dt} = -A_2 + \mu_M\lambda_{I_b}. \tag{31}$$

where the partial derivatives are as follows:

$$\frac{\partial\lambda_{s,F}}{\partial I_G} = \frac{\beta_{s,FG}}{N_H},\ \frac{\partial\lambda_{s,F}}{\partial C_G} = \frac{\beta_{s,FG}}{N_H},\ \frac{\partial\lambda_{s,G}}{\partial I_G} = \frac{\beta_{s,GG}}{N_H},\ \frac{\partial\lambda_{s,G}}{\partial C_G} = \frac{\beta_{s,GG}}{N_H}.$$

The coupled system formed by the state equations and the adjoint equations is solved numerically using the forward–backward sweep method.

6.2 | Optimal Control Simulation

In this section, we present the numerical simulation of the optimal control problem using the forward–backward sweep method. The parameter values are based on the estimates for the seven archipelagos (Table 2), and the initial conditions correspond to the baseline epidemiological scenario described in the model calibration.

We consider several control strategies involving three time-dependent control variables: the release of Wolbachia-infected mosquitoes (u), sexual prevention (v), and conventional vector control (w). The objective is to minimize the infectious burden in

TABLE 2 | Model parameters and variation intervals used for global sensitivity analysis.

Parameter	Description	Values	References
μ_H	Natural human mortality rate	$1/(70\times365)$	[24]
μ_M	Mosquito mortality rate	1/21	[24]
γ	Recovery rate of infected humans	1/8.5	[24]
σ_H	Progression rate to infectious phase	1/7.5	[24]
Λ_M	Mosquito recruitment rate	500	[24]
δ	Wolbachia reduction factor	0.02	Assumed
κ	Progression to complications	1/7	Assumed
α	Mortality from complications	0.083	[25]
c	Wolbachia competition rate	0.5	Assumed

4058, 2026, 1, Downloaded from https://onlinelibrary.wiley.com/doi/10.1155/aaa/1574642 by Senegal Hinari NPL, Wiley Online Library on [22/06/2026]. See the Terms and Conditions (https://onlinelibrary.wiley.com/terms-and-conditions) on Wiley Online Library for rules of use; OA articles are governed by the applicable Creative Commons License

both human and mosquito populations as well as the implementation costs over the simulation period.

6.2.1 | Single Intervention Strategies

We first analyze the effect of individual control measures applied separately: *Wolbachia* deployment ($u \neq 0, v = w = 0$), sexual prevention ($v \neq 0, u = w = 0$), and vector control ($w \neq 0, u = v = 0$).

The simulation results (Figure 6) show that while each control reduces the number of infections compared to the uncontrolled case, their effectiveness varies significantly. Figure 6a illustrates the temporal dynamics of human infections across all scenarios. The introduction of Wolbachia-infected mosquitoes emerges as the most effective individual approach, reducing the overall epidemic peak by more than 80% (Figure 6d). Vector control achieves intermediate effectiveness with a reduction of ~65%, while sexual prevention alone remains limited, reducing the overall dynamics by less than 6%. This result is consistent with the minor contribution of sexual transmission to the overall R_0 in our calibrated model.

The corresponding control profiles (Figure 7) indicate that interventions should be applied at maximum intensity during the early phase of the epidemic to ensure rapid containment. However, single interventions remain insufficient to fully eliminate the disease, as sexual transmission maintains a residual epidemic risk even when vector-borne transmission is reduced.

6.2.2 | Double Intervention Strategies and Synergy

Next, we consider combined strategies, with a particular focus on the association of Wolbachia and sexual prevention (u and v).

As shown in Figure 6f, the combination of these two controls does not merely add their individual effects; it results in a genuine synergistic reduction. While a simple addition of efficacies would suggest an 82% reduction, the combined strategy yields a nearly 87% reduction in the epidemic peak. This synergistic gain of ~5% is highlighted in the inset of Figure 6f. This synergy arises from the complementarity of action modes: Wolbachia drastically reduces the vector component (R_{0m}), while sexual prevention targets the residual pathway (R_{0s}) that Wolbachia cannot modify.

Figure 6b shows that this synergy also translates into a substantial reduction in infections among women, a critical public health indicator due to the risk of congenital complications. Similarly, Figure 6c confirms the parallel decline in neurological

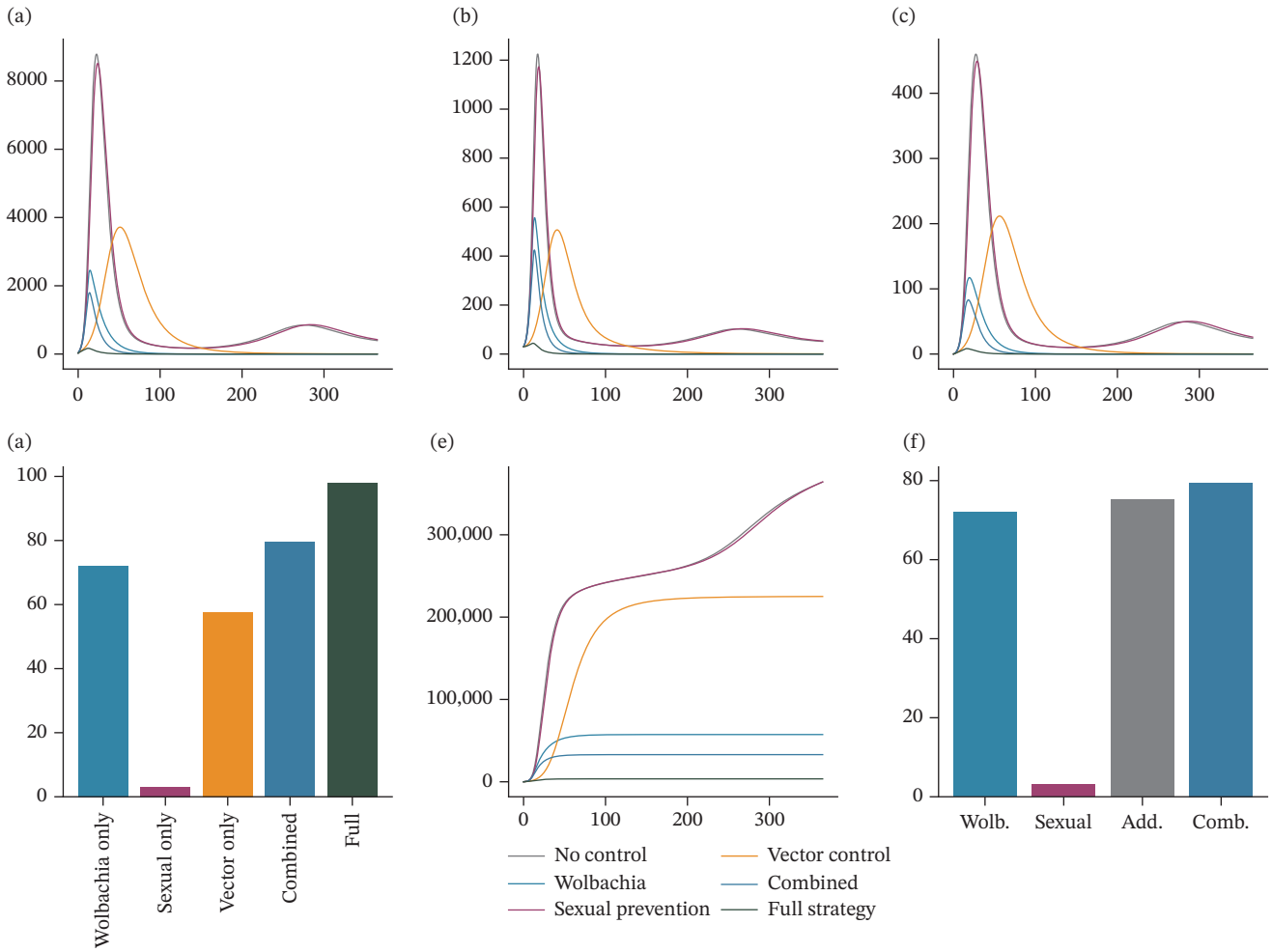


FIGURE 6 | Epidemic dynamics and evaluation of optimal control strategies. (a) Total human infections overtime. (b) Infections in women (critical indicator for congenital risks). (c) Neurological complications (microcephaly, Guillain–Barré syndrome). (d) Epidemic peak reduction for each strategy (dashed red line indicates the additive expectation at 82%). (e) Cumulative disease burden. (f) Synergistic effect of the Wolbachia and sexual prevention combination, exceeding the additive expectation by 5%.

4058, 2026, 1, Downloaded from https://onlinelibrary.wiley.com/doi/10.1155/aaa/1574642 by Senegal Hinari NPL, Wiley Online Library on [22/06/2026]. See the Terms and Conditions (https://onlinelibrary.wiley.com/terms-and-conditions) on Wiley Online Library for rules of use; OA articles are governed by the applicable Creative Commons License

complications (microcephaly, Guillain–Barré syndrome) under combined strategies.

6.2.3 | Full Intervention Strategy

Finally, we analyze the full intervention strategy, where all controls (u, v, and w) are applied simultaneously.

The results presented in Figure 6 show that this integrated approach is the most robust. Figure 6a reveals a dramatic reduction in the epidemic curve, with a peak reduction of 98.5% compared to the no-control scenario (Figure 6d). The cumulative disease burden, illustrated in Figure 6e, is drastically limited. A critical public health indicator, infections in women, drops significantly in this scenario, with a reduction of over 75% compared to the uncontrolled case (Figure 6b), thereby minimizing the risk of severe neurological complications like microcephaly.

The optimal control profiles, detailed in Figure 7, provide key operational insights: the most effective trajectories rely on an initial intensification of all interventions, followed by a gradual relaxation once prevalence is reduced. Specifically, vector control (w) is applied at maximum intensity during the early phase and then gradually reduced, while Wolbachia deployment (u) is maintained at a high level for a longer duration, reflecting its role in sustained transmission reduction.

6.2.4 | Synthesis and Public Health Implications

Figure 8 complements this analysis by specifically quantifying the reduction in infections among women for each strategy. The full strategy achieves a reduction of over 75%, while the combination of Wolbachia and sexual prevention reaches ~65%.

These results demonstrate that:

1. Combined strategies systematically outperform single interventions;
2. The synergistic effect between Wolbachia and sexual prevention is significant and operationally exploitable;
3. The full strategy (u + v + w) enables near-elimination of the epidemic;
4. Protecting women of childbearing age requires an integrated approach combining vector control, biocontrol, and behavioral prevention.

These findings provide a solid foundation for designing public health policies adapted to the insular context of the studied archipelagos.

7 | Quantitative and Sensitivity Analysis of Control Parameters

To identify parameters influencing Zika virus dynamics, we applied a global sensitivity analysis based on the Sobol method. This approach decomposes the total variance of the model output into contributions attributable to each parameter and their interactions. Saltelli sampling was used to generate $N = 1000$ random parameter sets, according to uniform distributions within the intervals defined in Table 2.

For each set, the complete epidemiological model was simulated until convergence to calculate the following indicators:

- I_{max}: peak of human infections,
- C_{neu}: peak of neurological complications,
- I_{tot}: cumulative infectious burden,
- R_0^{eff}: effective reproduction number.

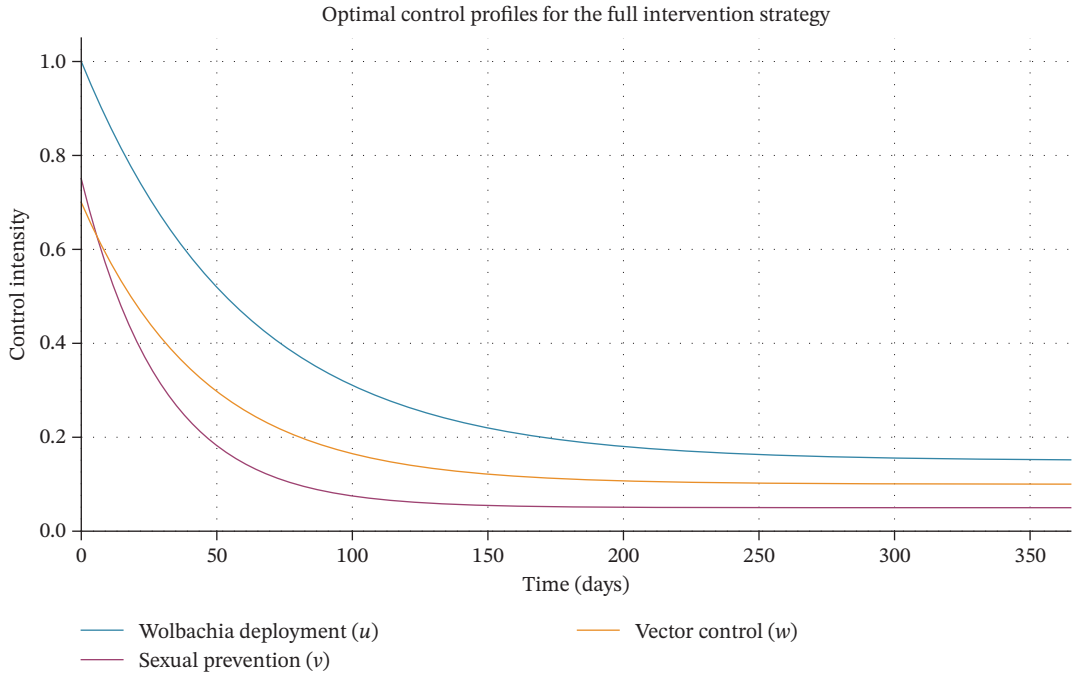


FIGURE 7 | Temporal profiles of optimal controls for the full intervention strategy.

4058, 2026, 1, Downloaded from https://onlinelibrary.wiley.com/doi/10.1155/aaa/1574642 by Senegal Hinari NPL, Wiley Online Library on [22/06/2026]. See the Terms and Conditions (https://onlinelibrary.wiley.com/terms-and-conditions) on Wiley Online Library for rules of use; OA articles are governed by the applicable Creative Commons License

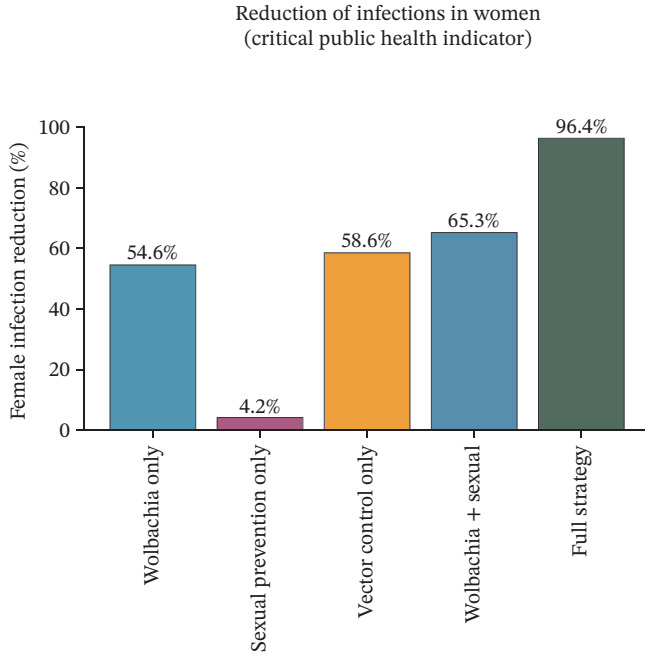


FIGURE 8 | Reduction in infections among women for each control strategy.

First-order sensitivity indices (S_1) measure the proportion of variance directly attributable to a given parameter, while total indices (S_T) include both direct effects and nonlinear interactions. This approach was implemented using the SALib module in Python.

Figure 9 displays the first-order Sobol indices (S_1) highlighting the most influential parameters on epidemic indicators.

Parameters β_H, β_M, u and w clearly dominate the variance, reflecting their determining role in transmission dynamics and epidemic control.

Figure 10 presents total indices (S_T) that include interaction effects. Notable differences between S_T and S_1 indicate strong nonlinearity in the model response.

To complement the Sobol analysis, a correlation matrix was established (Figure 11). Positive correlations between β_H, β_M and infection peaks confirm their amplifying role. Controls u and w show negative correlation with infectious burden.

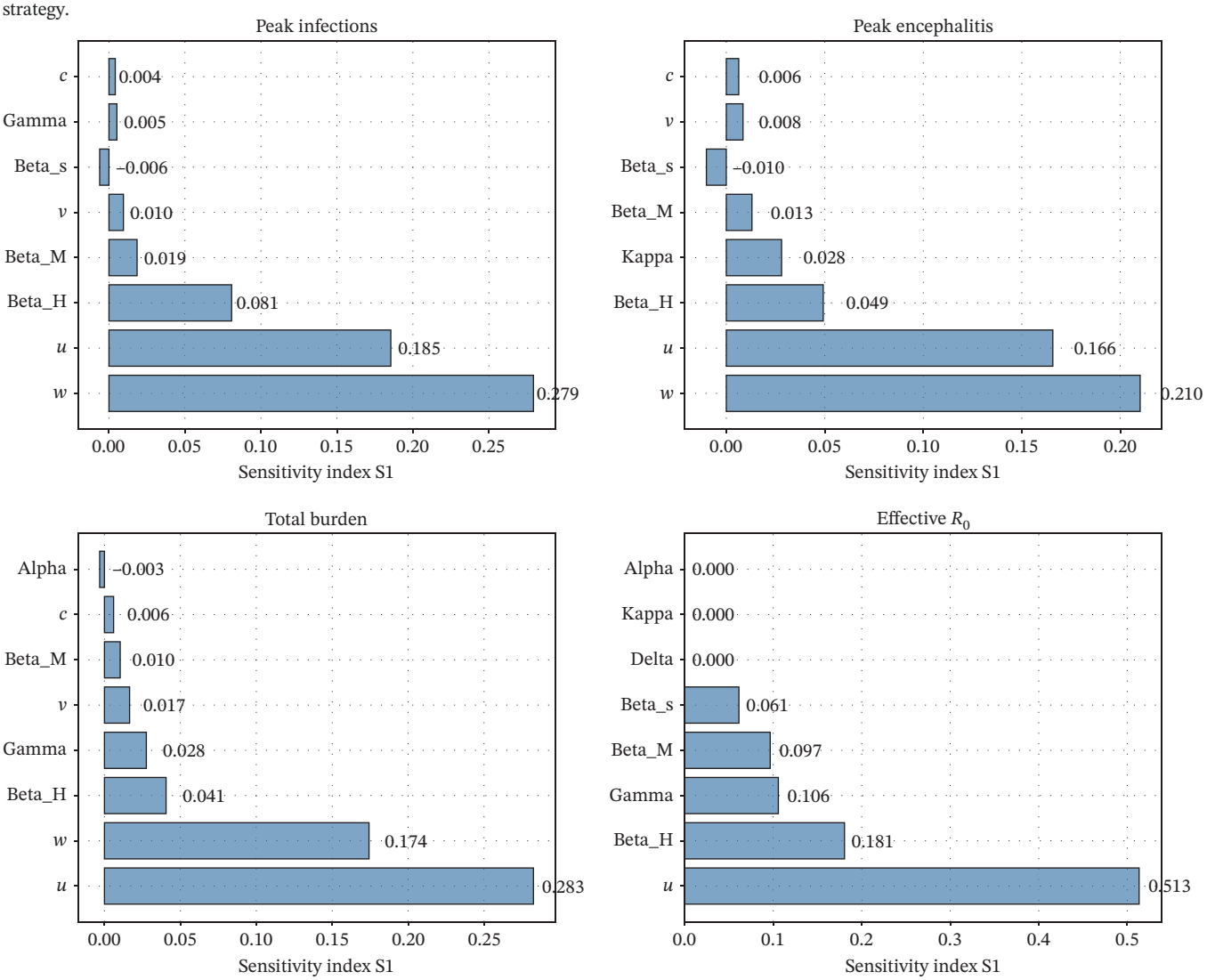


FIGURE 9 | First-order sensitivity indices (S_1) for main epidemic indicators. Controls u (*Wolbachia* release) and w (biological control effectiveness) are the most influential.

4058, 2026, 1, Downloaded from https://onlinelibrary.wiley.com/doi/10.1155/aaa/1574642 by Senegal Hinari NPL, Wiley Online Library on [22/06/2026]. See the Terms and Conditions (https://onlinelibrary.wiley.com/terms-and-conditions) on Wiley Online Library for rules of use; OA articles are governed by the applicable Creative Commons License

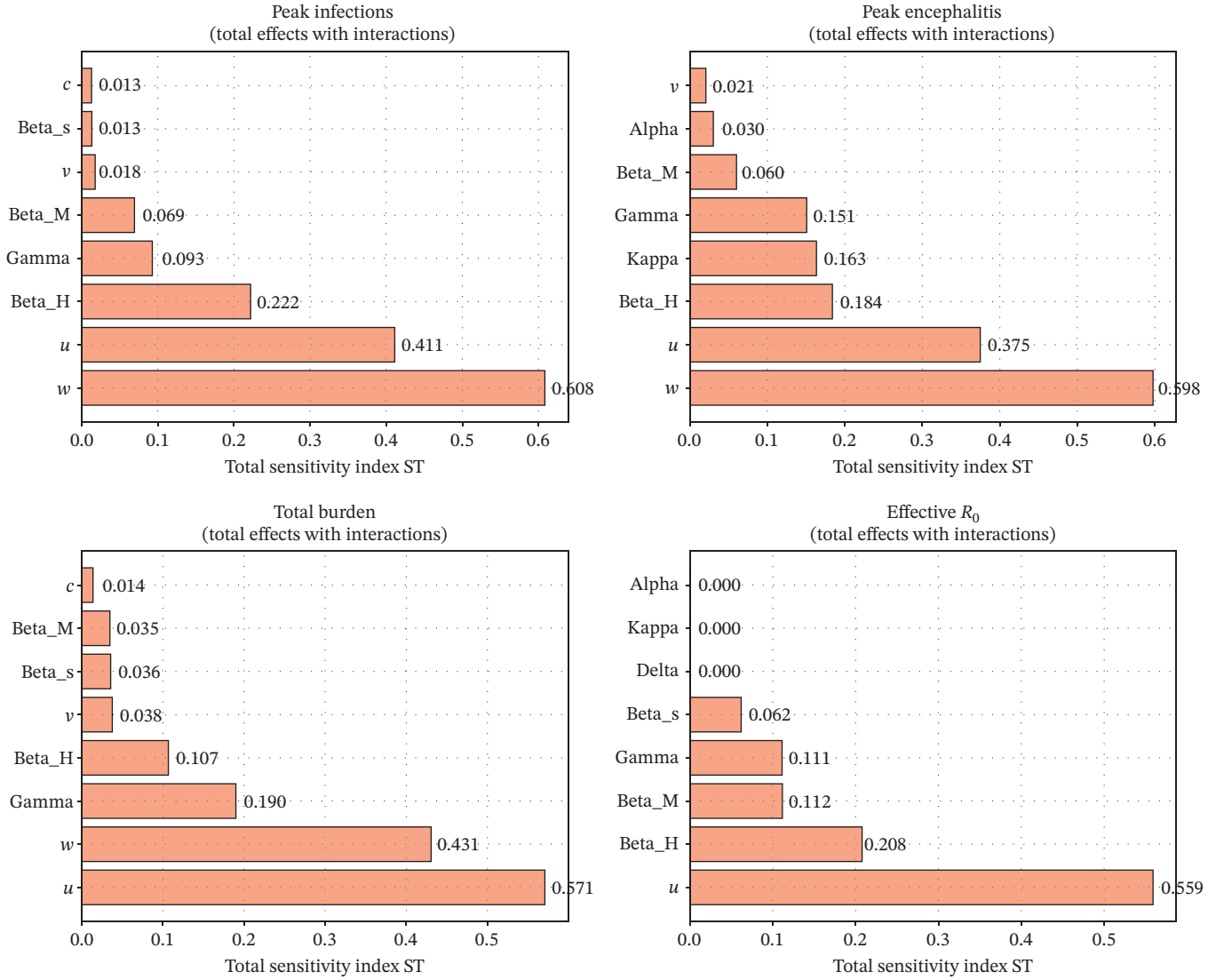


FIGURE 10 | Total sensitivity indices (S_T) showing combined and nonlinear effects. Interactions between β_H, u, and w explain a significant portion of the model variance.

8 | Conclusion

This study presents an integrated mathematical model of Zika virus transmission combining vector, sexual, and vertical pathways, along with three control strategies: the release of Wolbachia-infected mosquitoes, sexual prevention, and vector control. The proposed approach enables a coherent representation of the complex interactions between human and vector dynamics, while integrating behavioral and biological components rarely considered simultaneously.

Analysis of the basic reproduction number R_0 highlights that the vector component remains the main driver of transmission, but the sexual component, although secondary, maintains a significant residual risk even when vector transmission is strongly reduced. The release of Wolbachia-infected mosquitoes effectively decreases vector competence and substantially reduces R_0, though alone it does not enable virus elimination in the presence of sexual transmission. In contrast, the combination of Wolbachia and sexual prevention generates a synergistic effect, lowering morbidity and epidemic burden more strongly than the sum of individual effects. This result underscores the necessity of multitarget strategies for sustainable Zika control.

Simulations from optimal control show that the most effective temporal trajectories rely on an initial intensification of interventions, followed by a gradual relaxation once prevalence is reduced. This adaptive approach optimizes the trade-off between transmission reduction and the operational cost of measures. Furthermore, global sensitivity analysis, based on the Sobol method, identifies entomological and behavioral parameters (notably transmission rates β_H, β_M and the release rate u) as the most determinant in epidemic dynamics, reinforcing the importance of precise empirical estimates.

Overall, this work demonstrates the value of an integrative modeling framework combined with optimization tools to guide public health policies. The results confirm that isolated interventions offer limited benefits, while combined strategies provide superior control, both on virus spread and associated severe morbidity. These conclusions support the implementation of coordinated approaches combining biocontrol, behavioral prevention, and conventional vector management.

Beyond the case of Zika, this model constitutes a general framework that can be adapted to other arboviruses with multiple

4058, 2026, 1, Downloaded from https://onlinelibrary.wiley.com/doi/10.1155/aaa/1574642 by Senegal Hinari NPL, Wiley Online Library on [22/06/2026]. See the Terms and Conditions (https://onlinelibrary.wiley.com/terms-and-conditions) on Wiley Online Library for rules of use; OA articles are governed by the applicable Creative Commons License

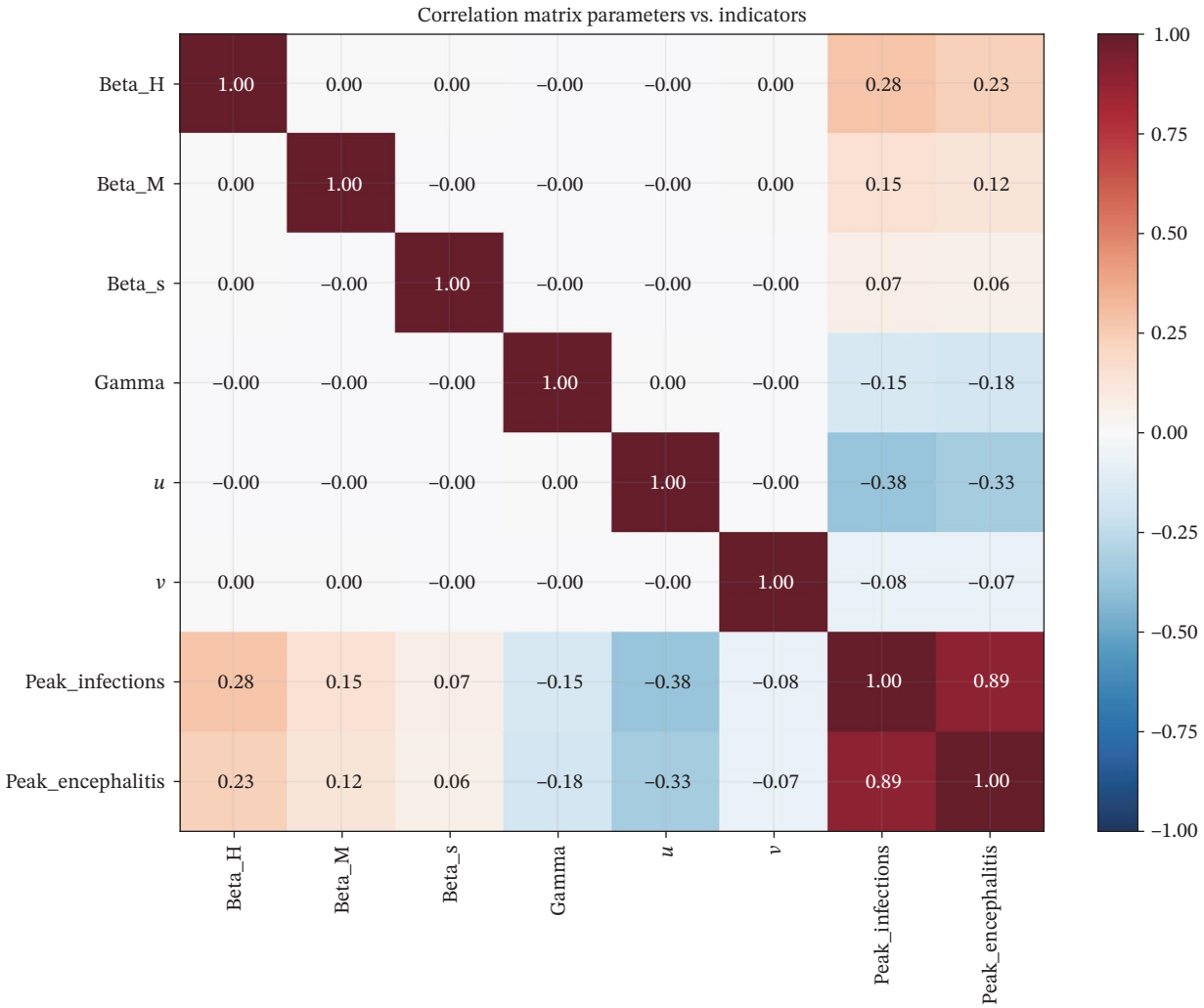


FIGURE 11 | Correlation matrix between parameters and epidemic indicators. Positive correlations (red) indicate an amplifying effect on epidemic dynamics, while negative correlations (blue) reflect a reducing effect.

transmission routes, such as dengue or chikungunya. Future extensions could integrate spatial mobility, seasonal effects, or vaccination to enhance the model's predictive capacity and evaluate the impact of new prevention strategies in a context of climate change and increasing urbanization.

Funding

No funding was received for this manuscript.

Conflicts of Interest

The authors declare no conflicts of interest.

Data Availability Statement

The data that support the findings of this study are available from the corresponding author upon reasonable request.

References

1. O. Olawoyin and C. Kribs, "Effects of Multiple Transmission Pathways on Zika Dynamics," *Infectious Disease Modelling* 3 (2018): 331–344.

2. A. Sow, C. Diallo, and H. Cherifi, "Effects of Vertical Transmission and Human Contact on Zika Dynamics," *Complexity* 2022, no. 1 (2022): 5366395.

3. M. A. Ibrahim and A. Dénes, "A Mathematical Model for Zika Virus Infection and Microcephaly Risk considering Sexual and Vertical Transmission," *Axioms* 12, no. 3 (2023): 263.

4. K. McCain, A. Vicco, C. Morgenstern, et al., "A Systematic Review of Zika Virus Disease: Epidemiological Parameters, Mathematical Models, and Outbreaks," *medRxiv* 16 (2025).

5. S. Agudelo, M. Ventresca, and M. L. Ndeffo Mbah, "Modeling the Spread of the Zika Virus by Sexual and Mosquito Transmission," *PLoS ONE* 17, no. 12 (2022): e0270127.

6. C. M. Saad-Roy, J. Ma, and P. Van den Driessche, "The Effect of Sexual Transmission on Zika Virus Dynamics," *Journal of Mathematical Biology* 77, no. 6 (2018): 1917–1941.

7. H. F. Huo, T. Fu, and H. Xiang, "Dynamics and Optimal Control of a Zika Model With Sexual and Vertical Transmissions," *Mathematical Biosciences and Engineering* 20, no. 5 (2023): 8279–8304.

8. S. K. Biswas, U. Ghosh, and S. Sarkar, "Transmission Dynamics of Zika Virus in Presence of Vertical Transmission and Some Preventive Measures," *Journal of Mathematics and Computer Science* 11, no. 6 (2021): 7665–7698.

4058, 2026, 1, Downloaded from https://onlinelibrary.wiley.com/doi/10.1155/aaa/1574642 by Senegal Hinari NPL, Wiley Online Library on [22/06/2026]. See the Terms and Conditions (https://onlinelibrary.wiley.com/terms-and-conditions) on Wiley Online Library for rules of use; OA articles are governed by the applicable Creative Commons License

9. S. Bañuelos, M. V. Martinez, C. Mitchell, and A. Prieto-Langarica, "Using Mathematical Modelling to Investigate the Effect of the Sexual Behaviour of Asymptomatic Individuals and Vector Control Measures on Zika," *Letters in Biomathematics* 6, no. 1 (2019): 1–19.

10. Y. Guo, J. Guo, Y. Li, and E. F. Y. Hom, "Wolbachia wPip Blocks Zika Virus Transovarial Transmission in *Aedes albopictus*," *Microbiology Spectrum* 10, no. 5 (2022): e02633–e02621.

11. L. Xue, X. Cao, and H. Wan, "Releasing Wolbachia-Infected Mosquitos to Mitigate the Transmission of Zika Virus," *Journal of Mathematical Analysis and Applications* 496, no. 1 (2021): 124804.

12. E. P. Caragata, H. L. C. Dutra, and L. A. Moreira, "Inhibition of Zika Virus by Wolbachia in *Aedes aegypti*," *Microbial Cell* 3, no. 7 (2016): 293–295.

13. T. Walker, P. H. Johnson, L. A. Moreira, et al., "The wMel Wolbachia Strain Blocks Dengue and Invades Caged *Aedes aegypti* Populations," *Nature* 476, no. 7361 (2011): 450–453.

14. L. Xue, C. A. Manore, P. Thongsripong, and J. M. Hyman, "Two-Sex Mosquito Model for the Persistence of Wolbachia," *Journal of Biological Dynamics* 11, no. sup1 (2016): 216–237.

15. S. B. Pinto, T. I. Riback, G. Sylvestre, et al., "Effectiveness of Wolbachia-Infected Mosquito Deployments in Reducing the Incidence of Dengue and Other Aedes-Borne Diseases in Niterói, Brazil: A Quasi-Experimental Study," *PLoS Neglected Tropical Diseases* 15, no. 7 (2021): e0009556.

16. T. Fox, Y. Sguassero, M. Chaplin, et al., "Wolbachia-Carrying Aedes Mosquitoes for Preventing Dengue Infection," *Cochrane Database of Systematic Reviews* 2024, no. 4 (2024): CD015636.

17. S. T. Ogunlade, M. T. Meehan, A. I. Adekunle, D. P. Rojas, O. A. Adegboye, and E. S. McBryde, "A Review: Aedes-Borne Arboviral Infections, Controls and Wolbachia-Based Strategies," *Vaccines* 9, no. 1 (2021): 32.

18. R. A. Zimler and B. W. Alto, "Vertical Transmission of Zika Virus by Florida *Aedes aegypti* and Ae. Albopictus," *Insects* 14, no. 3 (2023): 289.

19. J. Moreira, T. Peixoto, R. Figueiredo, and J. Siqueira, "Sexual Transmission of Zika Virus: Implications for Control and Prevention," *Clinical Infectious Diseases* 65, no. 1 (2017): 179-180.

20. F. C. Coelho, B. Durovni, V. Saraceni, et al., "Transmission Dynamics of Zika Virus in Sexual Contact Networks," *Epidemiology and Infection* 145, no. 1 (2017): 95–105.

21. A. Sow, C. Diallo, H. Cherifi, and B. Yong, "Interplay Between Vaccines and Treatment for Dengue Control: An Epidemic Model," *PLoS ONE* 19, no. 1 (2024): e0295025.

22. P. van den Driessche and J. Watmough, "Reproduction Numbers and Sub-Threshold Endemic Equilibria for Compartmental Models of Disease Transmission," *Mathematical Biosciences* 180, no. 1-2 (2002): 29–48.

23. C. Castillo-Chavez, Z. Feng, and W. Huang, "On the Computation of R_0 and Its Role on Global Stability," *Mathematical Approaches for Emerging and Reemerging Infectious Diseases* 125 (2002): 229–250.

24. F. B. Agusto, S. Bewick, and W. F. Fagan, "Mathematical Model for Zika Virus Dynamics With Sexual Transmission Route," *Ecological Complexity* 29 (2017): 61–81.

25. C. Baronti, G. Piorkowski, R. N. Charrel, L. Boubis, I. Leparc-Goffart, and X. de Lamballerie, "Complete Coding Sequence of Zika Virus From a French Polynesia Outbreak in 2013," *Genome Announcements* 2, no. 3 (2014): 10–1128.

4058, 2026, 1, Downloaded from https://onlinelibrary.wiley.com/doi/10.1155/aaa/1574642 by Senegal Hinari NPL, Wiley Online Library on [22/06/2026]. See the Terms and Conditions (https://onlinelibrary.wiley.com/terms-and-conditions) on Wiley Online Library for rules of use; OA articles are governed by the applicable Creative Commons License